Ice motion and driving forces during a spring ice shove on the Alaskan Chukchi coast

Andrew MAHONEY,[1] Hajo EICKEN,[1] Lewis SHAPIRO,[1] Tom C. GRENFELL[2]
[1]*Geophysical Institute, University of Alaska Fairbanks, Fairbanks, Alaska 99775, U.S.A.*
E-mail: Mahoney@gi.alaska.edu
[2]*Department of Atmospheric Sciences, University of Washington, Box 351640, Seattle, Washington 98195-1640, U.S.A.*

ABSTRACT. An ice shove along the Alaskan Chukchi Sea coast occurred in June 2001, affecting the communities of Barrow and Wainwright, some 150 km apart. Aerial photography before and after the event allowed measurement of ice displacement vectors near Barrow where up to 395 m of ice motion was accommodated almost entirely in discrete ridges up to 5 m high. The forces required to build these ridges are estimated at 35–62 kN m^{-1}, and driving forces of the whole event are investigated. Most ice deformation at or near the beach coincided with local onshore winds, but the event was preceded by the compaction of pack ice in the central Chukchi Sea and the closure of the coastal flaw lead, driven by the larger-scale wind field acting over several days beforehand. Whether this acted to impart pack-ice stress to the coast or simply to create a critical fetch of consolidated ice is uncertain. The near-melting near-isothermal state of the ice may have been a complicit factor and affected the behavior of the land-fast ice. Coastal morphology and bathymetry affected the location of deformation. This study highlights the range of scales at which processes act and culminate to have implications for Arctic communities.

1. INTRODUCTION

Deformation of sea ice is a nearly continual process in the Arctic as wind and ocean currents force the ice cover to converge or diverge. The implications of this are many and far-reaching, such as the creation of open water leading to rapid new-ice production in winter and the generation of thicker, summer-enduring multi-year ice. However, it is in the land-fast ice, which is attached to the coast, that such dynamics intimately affect humans.

Convergent, dynamic events in the sea ice are commonly called ice shoves in the literature or *ivu* in the singular by the Iñupiat Eskimos of northern Alaska. They occur throughout the ice cover and episodically in the littoral zone where they can affect coastal communities by impeding travel and potentially threatening infrastructure and lives. Ice shoves in the littoral zone are also capable of reworking beach material, so their implications for coastal sediment processes, in particular barrier island morphology, should not be overlooked (Reimnitz and others, 1990).

The onshore motion of the land-fast ice during a shove event is principally accommodated by two modes of deformation, often termed "onshore ride-up" and "onshore pile-up" (e.g. Kovacs and Sodhi, 1980; Sodhi and others, 1983). In the former case, ice advances up the beach and sometimes several hundred meters over land as a largely intact sheet (Brower, 1960). The latter case involves the building of a ridge of broken blocks of ice at the beach and little encroachment onto land.

These two processes are analogous to rafting and ridging in pack ice. Hopkins and others (1999) show the mode of deformation adopted by two converging floes is a function of ice-thickness distribution, with the likelihood of rafting decreasing as ice thickness and thickness heterogeneity increase. Studies of pack-ice deformation (Parmerter, 1975; Hopkins and others, 1999) have suggested that more force is required and energy expended in rafting ice than in forming ridges, meaning that the large-scale strength of the ice is higher if the conditions predispose it to raft rather than ridge-build. Work by Sodhi and others (1983) suggests that beach slope and roughness determine whether the ice piles at the beach or rides up the beach.

Ice shoves occur in land-fast ice when an onshore force is applied and conditions are such that the land-fast ice moves and deforms. Force is required to overcome the gravitational forces associated with the weight or buoyancy of the ice when moving it up a beach or building a ridge. Additional force is required to overcome dissipative forces, which include friction at sliding interfaces and those involved in bending, buckling and breaking the ice. The magnitudes of the dissipative forces are dependent on the mechanical properties of the ice and on the way in which it deforms or fails, but are dominated by frictional dissipation.

The force applied to the land-fast ice at any instant must be greater than the sum of the gravitational and dissipative forces, and the ice offshore must be sufficiently strong to transmit this force. The ice is held fast to land by frozen, bottom-fast ice and grounded floes and ridges, suggesting that melting and uplift of the land-fast ice are complicit mechanisms in some ice shoves. Attempting to calculate these forces from first principles is a formidable task when the processes involved are not fully quantifiable. We use the work of other authors together with measurements and observations before, during and after an onshore ice shove

Table 1. Timeline of events and data gathered in this study

Date	*Event*	*Field observations by authors*	*Ice mass-balance measurements*	*Aerial photography*	*Satellite remote-sensing data*	*Weather data*
19–30 May	Land-fast ice thickness, salinity and morphology mapping	•				
31 May	Maximum ice thickness achieved and onset of melt	•	•		•	•
8 June	Flaw lead open		•		•	•
11 June	Onshore winds, lead closing		•	•	•	•
13 June	Convergence in nearshore ice		•	•		•
14 June	Onshore winds. Shore lead closed. ~ 5 m ice ride-up at beach	•	•	•	•	•
15 June	Brief, minor episodes of ice motion at beach. Southwest–southeast winds	•	•	•		•
18 June	Onshore winds. ~ 45 m of ice motion at beach, with further deformation offshore	•	•		•	•
22 June	Flaw lead opens	•		•		•

near Barrow in June 2001 to determine order-of-magnitude estimates of the forces involved.

Previous work has been done estimating ice forces for deformation of sea ice both in deep water and at beaches (Parmerter and Coon, 1972; Hopkins, 1994, 1997; Flato and Hibler, 1995). Hopkins (1997) compared output from a dynamic discrete-element model with results from laboratory experiments measuring the resultant forces active during an ice pile-up. Hopkins' model contains the most explicit treatment of friction between blocks building the ridge. Hopkins concedes that two-dimensionality in his model probably underestimates the total energy expended in ridge building, but claims better accuracy predicting the ratio between dissipative and gravitational forces, citing a value of 8.3 ± 1.

The impact of an ice shove upon a coast and its community depends upon whether the ice rides up the beach or piles up. Ice ride-ups represent greater threats to coastal infrastructure, whereas pile-ups can incorporate more sediment and hinder travel between the beach and land-fast ice. There have been many observations of onshore ice shoves in the Arctic, and, in their extensive survey of ice-shove literature, Kovacs and Sodhi (1980) report on shoves which consist entirely of ride-ups, entirely of pile-ups and in many cases of combinations of the two. There have been reports of onshore ice shoves at all times of the year when ice is present at the coast, though Kovacs and Sodhi note that they seem most common in fall and spring when the ice and weather are least stable.

The dynamic processes involved in ice shoves are inherently difficult to study due to their episodic nature. However, fortuitous timing of ongoing fieldwork and the occurrence of an ice shove near Barrow, Alaska, in June 2001 yielded an excellent opportunity for observing the motion and evolution of the land-fast ice before, during and after an ice shove.

This study improves our understanding of the forces required to drive an onshore ice shove and the response of land-fast ice to that forcing. By comparison with other compressive events at the coast when ice shoves did and did not occur, we emphasize the fact that there is a combination of several independent environmental factors necessary to initiate ice motion. Although a generalized set of requisite conditions remains elusive, we improve our capability to predict similar events in the future. In addition, the lessons learned about the mechanics of this onshore ice shove will be applicable to ice dynamics in general.

2. TIMELINE OF EVENTS AND DATA COLLECTION

Table 1 lists the sequence of events and types of data gathered for this study. Ice thickness, type, and ridge distributions were mapped approximately 2–3 weeks prior to the ice shove as part of routine field measurements for other ongoing studies of the land-fast ice at Barrow (Eicken and others, 2003). These data were later combined with satellite-borne synthetic aperture radar (SAR) data to describe the distribution and morphology of the land-fast ice prior to the ice shove.

Observations made on the ice and from satellite imagery show that the width of the land-fast ice prior to any move-

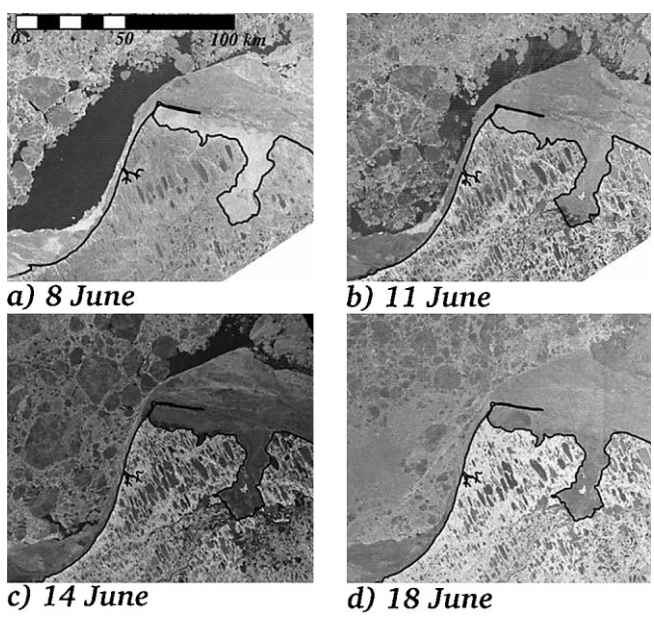

Fig. 1. RADARSAT SAR imagery over Barrow showing the nearshore ice in the days leading up to and during the ice shove. North is up.

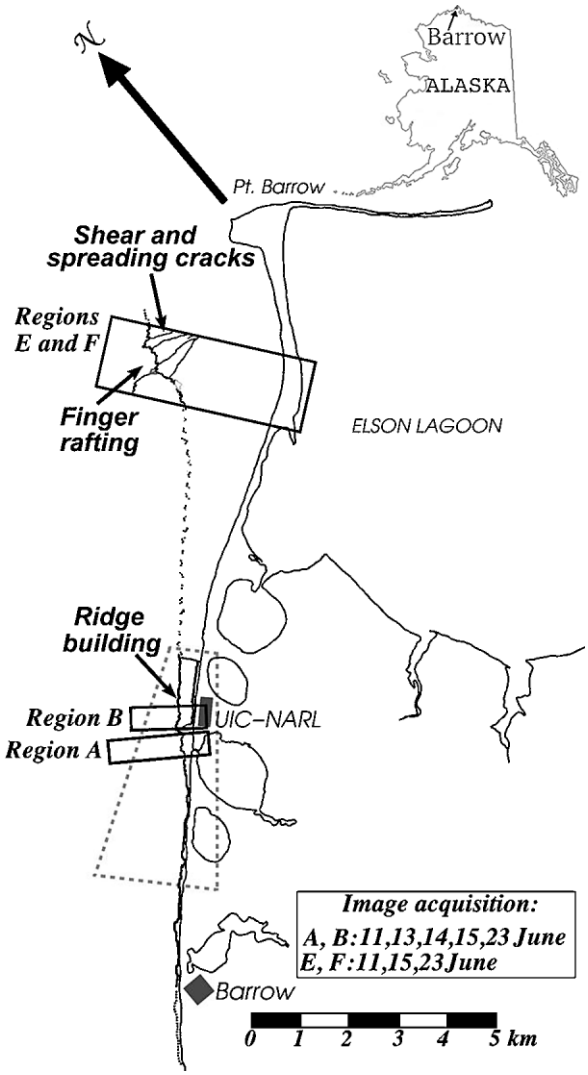

Fig. 2. Schematic plan view of the study area. Aerial photography provided coverage of most of the land-fast ice near Barrow on at least one occasion. The boxes show the regions for which co-registered mosaics were available on the listed dates. Also shown is the distribution of deformation features related to ice motion on 18 June. The dotted line represents the location of deformation inferred from oblique aerial photographs. The dashed quadrilateral at the lower left indicates the approximate ground coverage in Figure 5.

ment ranged from a minimum of approximately 3.5 km near Barrow to nearly 6 km near Point Barrow (Figs 1 and 2). Thirteen ice cores taken from the land-fast ice in late May indicate the ice cover consisted mostly of first-year ice. Only two cores had salinities in the upper 80 cm below 2 psu (practical salinity units), suggesting the existence of a few embedded floes of multi-year ice, although such low salinities could have occurred through drainage. In situ temperature measurements from instruments removed just prior to the ice shove suggest the ice sheet was above −2°C throughout.

Measurements of the land-fast ice thickness revealed that the ice was >1 m thick everywhere and up to 3.2 m thick in those floes assumed to be multi-year ice. Along the coast between the town of Barrow and the Ukpeagvik Inupiat Corporation–Naval Arctic Research Laboratory (UIC–NARL) (Fig. 2), areas of level first-year ice were confined to a strip within 100 m of the beach, beyond which the land-fast ice contained many ridges and regions of rubbled ice. Further northeast along the coast, however, in the shallow embayment of the spit of Point Barrow (Fig. 2), the ice was level over a large area up to 3 km from the shore.

The onset of melt occurred on 31 May and a moat started forming by melting of the bottom-fast ice zone (the region where the water is shallow enough that the ice freezes to the bed) within a few days. On 13 June it was observed that this moat had grown suddenly, possibly due to a local surge in sea level, though no hydrographic measurements exist at Barrow for this period. RADARSAT SAR imagery (Fig. 1) indicates there was a wide flaw lead beyond the offshore margin of land-fast ice on 8 June. By 14 June, the lead had closed and ground observations and aerial photographs show that it remained so until 22 June.

The land-fast ice first moved at the beach during the morning of 14 June, coinciding with onshore winds from the northwest as recorded at Barrow Wiley-Post Airport weather station, in Barrow (Fig. 3). This movement was sufficient to close the moat and cause buckling of the ice sheet (personal communication from R. Menge, 2001). The winds changed to southeast–southwest between 15 June and the afternoon of 18 June (Fig. 3), while short periods of minor deformation continued to occur, creating more buckling and modest ride-ups at the beach.

The majority of motion associated with the ice shove began between 1400 and 1700 h on 18 June, coinciding with the strongest local onshore winds of June. The movement lasted several hours, building ridges up to 5 m high at the beach and threatening equipment on the ice (personal communication from D. Perovich, 2001). More detailed observations of the features created during the ice shove were made after the termination of the event, including aerial photography and ground observations along the coast from just southwest of Barrow to approximately halfway along

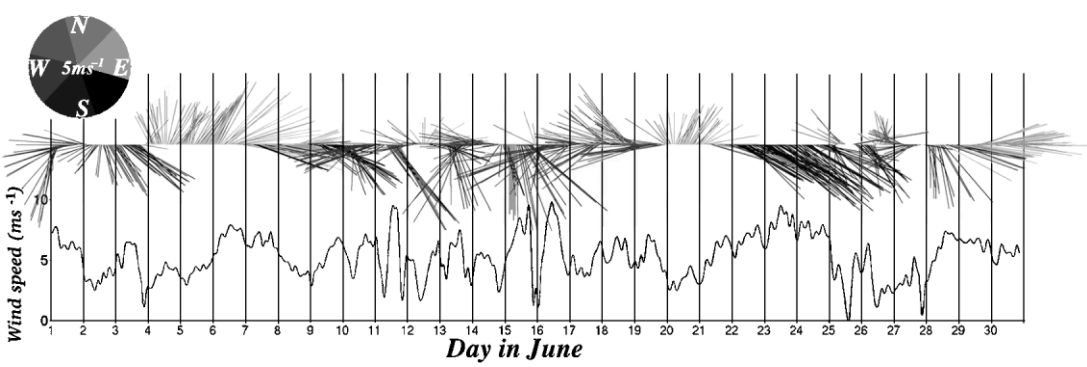

Fig. 3. Wind speed and direction for June 2001. Wind direction is shown by grayscale and direction of vectors. Wind speed is shown by length of vectors and the line plot beneath.

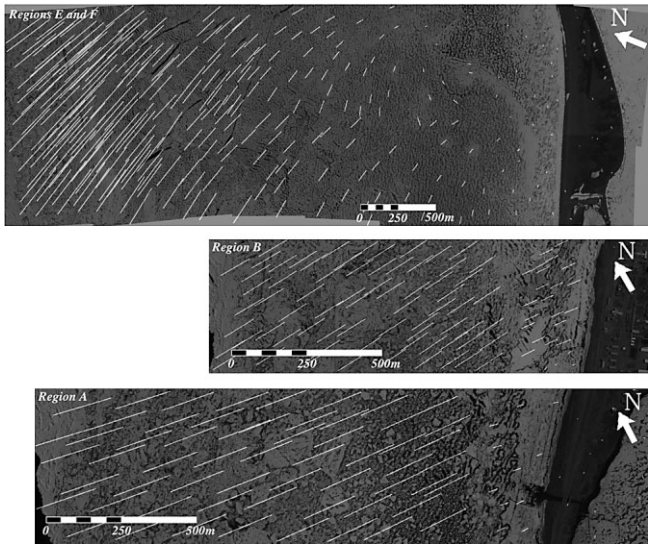

Fig. 4. Displacement vectors showing ice movement on 18 June as deduced from co-registered, mosaicked aerial photography on 15 and 23 June covering the regions shown in Figure 1. Ice motion was onshore, predominantly eastwards. Vectors are overlaid on 23 June mosaics, which have been darkened to improve the contrast.

the spit toward Point Barrow (Fig. 2). The extent and modes of deformation were noted and some sections of beach pile-up were profiled.

Fortuitously, swaths of the ice were being photographed from an aircraft throughout this period, as part of a study to monitor the evolution of the ice surface through the melt season (Eicken and others, in press). Overhead and oblique photography was available covering nearly the entire coast between Point Barrow and the town of Barrow. Overflights were made on 11, 13, 14, 15, 22 and 23 June, capturing the movement of the land-fast ice (Table 1). Images along each flight-line were stitched together where possible using PanaVue image mosaicking software and co-registered using identifiable features on the land.

Figure 2 illustrates the spatial and temporal coverage of subsets of this imagery where mosaicking and co-registration were possible. The flight-line-naming convention from Eicken and others (2004) is followed in this study. Flight-lines E and F were mosaicked together, but this was not possible for flight-lines A and B. We will refer to the subsets of the surface beneath flight-lines A, B, E and F as regions A, B, E and F respectively.

3. AERIAL PHOTOGRAPHY

Ice displacement was measured from the co-registered aerial imagery by picking features by eye that could be identified in consecutive images of the same region. This led to discrete displacement vector fields for each pair of subsequent mosaics for each region defined by irregularly spaced point measurements (Fig. 4). From these vector fields, the total motion at the beach and farther offshore in regions A, B, E and F was calculated.

There are many sources of potential error in the calculation of these vectors, including pitch and roll of the aircraft, errors in mosaicking, co-registration and pixel selection. An estimate of error magnitude was made by measuring displacement vectors of fixed terrestrial objects. These

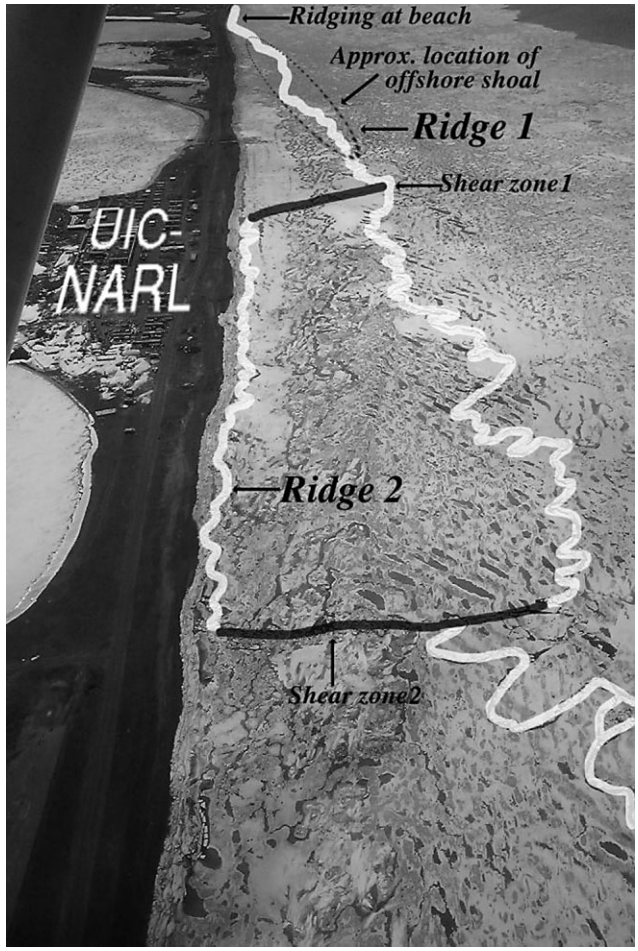

Fig. 5. Looking southwest over UIC–NARL, 23 June 2001, over ridges built during the ice motion on 18 June. Approximate ground coverage is indicated in Figure 2. Ridges are highlighted by sinuous white lines, and shear zones by gray lines, corresponding to black and gray lines respectively in Figure 2.

measurements yielded a mean apparent displacement error of 5 m with no trend in direction. In addition, displacement vectors from areas of ice that appeared to behave as rigid bodies, moving uniformly without deformation, showed deviations from their mean of similar magnitudes.

Errors associated with co-registration and mosaicking ought to increase offshore, with increasing distance from the reference points used on land. The data from all image pairs up to 15 June exhibit a linear increase in displacement magnitude with a gradient of around 0.02 m of apparent ice displacement per meter offshore, with no ridges or other evidence of deformation visible in the aerial photography. Thus any ice motion prior to 15 June was less than the collective errors in the measurements and so the following sections will focus on the displacement associated with the main event observed on 18 June. Field observations show that no comparable motion occurred between 15 and 23 June (Table 1) and so it is assumed that the images on these dates capture the motion of 18 June.

The displacement vectors calculated for regions E and F between 15 and 23 June also exhibit a near-linear increase in magnitude with increasing distance offshore, which initially suggests large mosaicking and co-registration errors. However, this increase begins several hundred meters offshore, which is compatible with the observation of no ridging at

or near the beach in this area (Fig. 4). Further, the aerial photographs show an increase in surface roughness beginning at approximately this distance offshore in the form of small (<50 m wide) discrete ridges. The motion required to build these features could yield an apparently continuous increase in the magnitude of the displacement vectors when the interval over which the motion field is sampled is greater than the transverse dimension of the ridges, as in this case.

4. RESULTS

4.1. Movement during the shove

As shown in Table 1, the first ice movement occurred during the morning of 14 June, but the majority of displacement and deformation occurred over a period of a few hours on 18 June. The total ice displacement observed at the beach before 18 June was approximately 5 m of ride-up as determined from concurrent and subsequent field observations. This initial ride-up, or evidence of it, was observed all along the beach between UIC–NARL and the town of Barrow (Fig. 2).

The calculated vectors of ice motion that occurred on 18 June in regions A and B (Fig. 4) indicate a net displacement, offshore from any ridges created in the land-fast ice, in the range of 140–175 m at an angle of about 50° with the shore. This displacement was accommodated at the sinuous ridges and a shear zone visible in the aerial photographs and shown obliquely from the air in Figure 5. This shear zone (shear zone 1 in Fig. 5) intersected a line of stakes previously frozen into the ice. This allowed a field measurement of the relative displacement across the shear zone of about 45 m, which agrees well with the calculated values of around 50 m in this area.

The vectors for regions E and F show up to 395 m of total displacement accommodated primarily along a sinuous region of deformation clearly visible in the aerial photographs, running approximately perpendicular to the ice motion. Ice displacement vectors for regions E and F were obtained over a larger area than regions A and B, which were limited by the position of the land-fast ice edge when the flaw lead reopened on 22 June. It is probable that deformation occurred further offshore from regions A and B in ice that was not captured by the aerial photography and later became detached from the coast. This could explain the large difference in total motion between regions A and B and regions E and F and highlights the difficulty in calculating the total land-fast ice motion.

4.2. Deformation of the land-fast ice

Deformation of the ice between 14 and 18 June resulted in approximately 5 m of beach ride-up and a ramped apron of ice on the beach, which was broken from the remaining ice sheet. The apron was visible where it was not buried beneath subsequently piled ice. This ice motion was small compared to the main event on 18 June and was not detectable on the aerial images, as discussed in section 3. The following discussion concentrates on the deformation that occurred on 18 June, although it is understood that the initial ride-up may have had an effect on the nature of the deformation that followed.

As shown in Figure 4, the ice displacement vectors for motion on 18 June are similar in direction in regions along the coast separated by several kilometers. However, the magnitude of the motion and the way in which it was accommodated differ significantly. From the ice displacement vector fields, it was possible to derive a strain field, indicating where and what manner of differential motion occurred.

This required interpolation of the original, irregularly sampled dataset to produce a dataset of regularly gridded displacement vectors. A modified linear inverse distance weighting method was adopted whereby the value at a mesh point of the interpolated grid was the average of a given number of nearest neighboring points from the original dataset, weighted by their respective distance from the mesh point. In the results presented below, a single nearest neighbor was used in the interpolations. This method effectively extends the area represented by an original data point until another is closer, causing no averaging or smoothing of the data.

Ridges were typically seen to occupy linear regions approximately 50 m wide, and all the ice displacement data were interpolated to a grid with 50 m between mesh points. This yielded approximately four times as many points as the original data, but with a single nearest neighbor the interpolation reflects the mechanics of the process if the deformation is assumed to occur within discrete regions separating other regions of no deformation.

The two principal orthogonal components of the two-dimensional strain field are given by (Thorndike, 1986)

$$E_{\mathrm{I}} = \frac{\partial u_x}{\partial x} + \frac{\partial u_y}{\partial y} \tag{1}$$

$$E_{\mathrm{II}} = \sqrt{\left(\frac{\partial u_x}{\partial y} - \frac{\partial u_y}{\partial x}\right)^2 + \left(\frac{\partial u_x}{\partial y} + \frac{\partial u_y}{\partial x}\right)^2}, \tag{2}$$

where u_x and u_y are the x and y components of the displacement vectors respectively. E_{I} is divergence, representing a change in area, with negative values implying a loss of area. E_{II} is the magnitude of the shear component, which represents deformation without change in area. With regularly gridded displacement vectors, the derivatives in Equations (1) and (2) can be approximated by a centered difference scheme. In these calculations, regions where ice motion was accommodated show up clearly (Fig. 6). Furthermore, regions of ice moving uniformly without deformation are also easily identified. These uniform areas are surprisingly extensive given the heterogeneous character of the land-fast ice away from the beach.

With a grid spacing of 50 m, a divergence or shear of 1 indicates a 50 m difference in displacement between adjacent points. The E_{I} and E_{II} fields for all regions show that the ice motion was almost exclusively taken up within discrete, linear regions that correspond to ridges and shear zones observed on the ground and in the aerial photographs and shown in Figure 2. Ridges at the beach continued southwest of Barrow as far as could be seen with binoculars, but were not clearly captured in any aerial photography.

The deformation that occurred near UIC–NARL, in regions A and B, is shown obliquely from the air in Figure 5. Onshore displacement of ice in these regions was accommodated by ridge building near and parallel to the beach. Four ridges and two shear zones are identified. The locations of the ridges and amount of ice motion accommodated by them appear to be governed to some extent by the presence of a shallow submarine shoal. Ridge 1 was formed above the shoal, accommodating approximately 125 m of ice

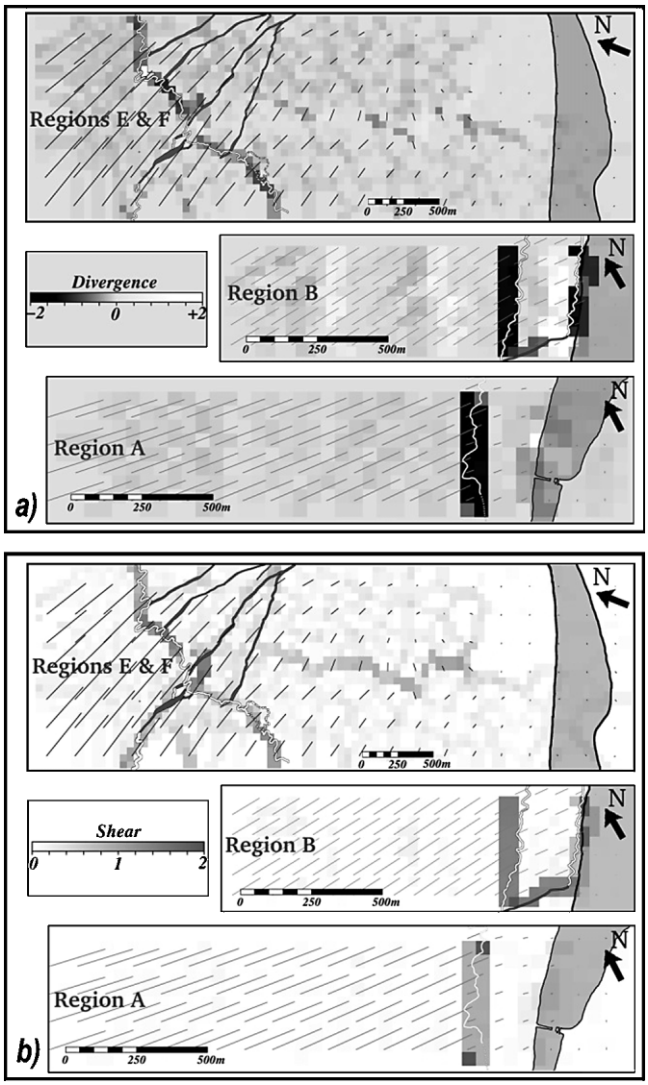

Fig. 6. Divergence (a) and shear (b) fields calculated from the motion vectors shown in Figure 4 regridded to a 50 m grid spacing. Regridded vectors are shown at 100 m grid spacing for regions A and B and 200 m grid spacing for regions E and F.

motion, leaving the ice at the beach almost undisturbed. Further north along the beach beyond the shoal, in region B, ridge 2 accommodated approximately 50 m of ice motion at the beach. Further offshore from ridge 2, ridge 3 accommodated around 60 m of ice motion. The shoal therefore is responsible for nullifying the impact of the ice shove upon the beach behind it and possibly reducing it in adjacent areas along the beach. The differential motion required at either end of ridge 2 was evident in the form of two shear zones sub-perpendicular to the coast.

Evidence of shear motion parallel to the beach was observed in the form of sets of en-echelon cracks and buckles in the ice over long stretches of the beach. The individual cracks varied in size but were typically tens of centimeters long, with openings of a few centimeters at the surface. The buckles were larger, rising approximately 0.5 m and being 2–3 m long. The orientation of these features agrees with the direction of the displacement vectors but they cannot account for the entire shore-parallel component of motion. It appears from Figure 6b that most of the shore-parallel component of motion was taken up by ridge building. Closer inspection of the aerial photographs reveals offsets on the ridges where such shear could be accommodated.

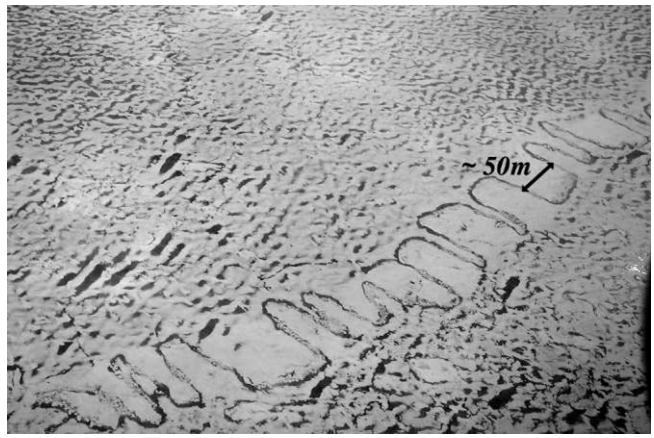

Fig. 7. The sinuous zone of ridging and rafting seen from the air near regions E and F. The lack of melt ponds within the zone suggests an elevated ice surface due to rafting.

The E_I and E_{II} fields for regions E and F show strong convergence and shear corresponding to the sinuous deformation zone approximately 2–3 km from the beach shown in black in Figure 2, in white with a black outline in Figure 6 and seen from the air in Figure 7. Though no surface observations were made in this region, the lack of melt ponds within the zone suggests an elevated ice surface caused by rafting or tilting. This is interpreted to be a zone of finger rafting, a phenomenon normally associated with thinner ice. The fingers are typically 50 m long and 10–50 m wide, with ridging evident at the ends, agreeing well with the 50–100 m of shortening measured from the aerial images.

Approximately perpendicular to the zone of finger rafting are cracks showing up to 25 m of spreading and up to 20 m of shear motion of different senses in the aerial photographs. They are shown in Figure 6b by gray lines beneath areas of shear, and the calculated shear values of 0.3–0.5 agree well with the values measured from aerial photographs. The rest of the ice in regions E and F shows higher convergence and shear values than the ice in regions A and B, resulting in the greater concentration of smaller ridges seen from the air. This is the only area where such diffuse deformation was apparent. The weak, linear feature across the center of the divergence and shear fields is attributed to mosaicking the two lines together because it does not correspond to any identifiable features in the images. The deformation-analysis results agree well with the observed lack of deformation at the beach in regions E and F.

4.3. Beach ridge morphologies

Variability in the behavior of the ice was observed on a variety of scales. At the smallest scale, there was much variability in the size of blocks into which the ice was broken, despite the fairly uniform thickness of the parent ice sheet. Along continuous sections of ridge at the beach, the ice was broken into blocks approximately 1 m on a side as well as into larger slabs of ice many meters across. This difference in block size manifested itself as differences in ridge height and morphology.

At the beach between shear zone 2 and the town of Barrow, the ridges varied in height between approximately 2 and 5 m and exhibited two distinct morphologies. The ridge labeled ridge 2 in Figure 5 was profiled at two points exem-

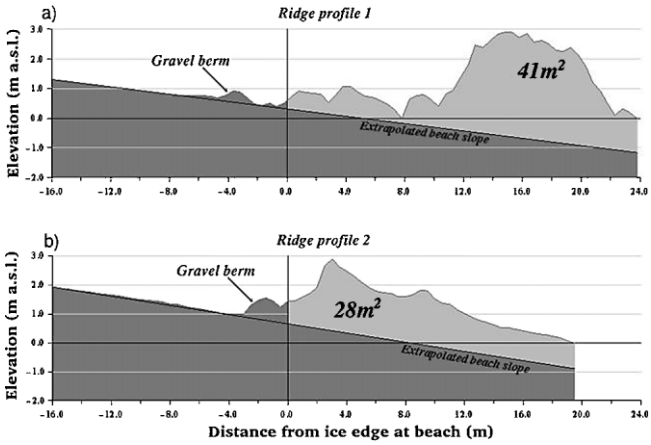

Fig. 8. Beach profiles showing two distinct morphologies: (a) rubble pile-up and (b) stacked rafts. The cross-sectional area is calculated by extrapolating the observed beach profile from above the ice.

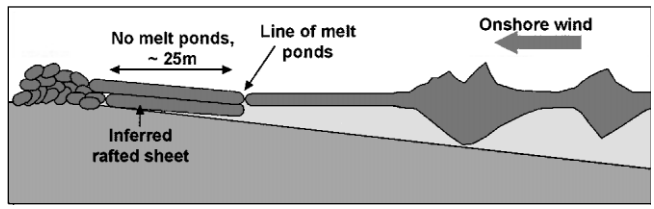

Fig. 9. Schematic of assumed distribution of ice in a cross section of the land-fast ice near the beach. Ridge building was observed and rafting was inferred from melt-pond patterns and discrepancies between ridge volume and ice displacement.

plifying these two morphologies (Fig. 8). Profile 1, with the larger cross-section of 41 m^2, typifies a section of beach where the ice broke into approximately cubic blocks, forming a steep-sided ridge a few meters offshore from the water's edge. Profile 2 has a cross-section of 28 m^2 and was taken across a section of ridge having the appearance of stacked slabs of ice, where larger pieces of ice had overridden each other to form a pile just above the waterline with a ramp-like offshore slope.

The ice in regions A and B, just offshore from UIC–NARL, was measured 3 weeks before the first ice motion (Table 1) and found to be 1.3–1.5 m thick. The blocks of ice contained within the ridges were typically about 1 m thick, when observed on 20 and 21 June. By taking the field measurement of 45 m of ice motion, we can make a conservative estimate of the volume of ice fed into the ridge, since we do not have an exact measurement of the initial ride-up distance on 14 June. Neither ridge profile contains enough ice, even assuming zero porosity, to accommodate 45 m onshore ice displacement, which amounts to 45 m^3 of ice per unit length of beach if we assume a uniform ice thickness of 1 m. The profiles span the width of the ridge that was visible above the surface, meaning there must be some form of deformation that was not apparent, more than can be accounted for by displacement of beach material or a reasonable steepening of the beach slope beneath the water. However, the absence of melt ponds in a region behind the ridge is again a clue, suggesting the occurrence of rafting and a double thickness of ice. This is shown schematically in Figure 9.

Such rafting would yield little noticeable effect on the surface topography beyond an increase in freeboard, which would not be visible from the surface, but would probably be enough to affect the drainage patterns leading to the absence of melt ponds seen from the air. This melt-pond-free region extended approximately 25 m offshore from the ridge and can be seen from UIC–NARL to the town of Barrow. If 25 m of onshore motion is accommodated in this fashion at both profiles, this accounts for all the ice and yields porosities of 51% and 29% for ridge profiles 1 and 2 respectively.

The potential energy stored in a ridge depends upon the mass of ice, which is inversely related to the porosity, multiplied by the elevation of that mass. The porosity value for ridge 1 seems high, probably because the elevation of the highest point on the ridge was used, rather than a lower elevation more representative of the pile-up (personal communication from A. Kovacs, 2003). However, this should not have a large effect on the calculated potential energy stored in a ridge, since an overestimation of ridge porosity will be balanced in part by a corresponding overestimation of ridge height. The potential energy stored in a ridge is calculated in section 5.1.

The causes of the observed differences in ice behavior and ridge morphology are unclear. However, the variability in ridge morphology agrees with the observations of Hopkins and others (1999) that there is a range of morphologies between those produced by pure ridging and pure rafting. It is therefore likely that the same conditions that determine these two processes were driving the difference in ridge morphology, i.e. ice thickness, thickness homogeneity and beach slope.

In addition to these differences in individual ridges, there were significant differences between the land-fast ice deformation in regions A and B and that in regions E and F. Although there were components of both rafting and ridging in both pairs of regions, a greater fraction of the ice motion in regions E and F was accommodated by rafting. This may be due to the greater homogeneity of ice thickness in this area, as stated in section 2.

Cracks, sub-parallel to the direction of ice motion and apparently radiating from a point, were also observed in regions E and F (shown in gray in Fig. 6) but not in regions A and B. The cracks have the appearance of spreading cracks under uniaxial compression where the ice was compressed against Point Barrow. However, this does not explain the apparent radial nature of the cracks, and other aerial photographs show similar patterns of cracks in the ice further northwest of Point Barrow.

Another way in which the ice deformation in regions A and B differs from that in regions E and F is in the location of the deformation with respect to the beach. In regions A and B the deformation took place at or near the beach, whereas in regions E and F it took place approximately 2–3 km offshore, leaving the ice at the beach undisturbed (Figs 2 and 4). Without good knowledge of the distribution of stress applied to the land-fast ice and the distribution of flaws, it is impossible to predict where the ice ought to fail. Figure 2 suggests there is a relationship between the curvature of the coast and the location of deformation. In the concave curve of the spit of Point Barrow, the deformation occurred offshore, whereas where the coastline was straight or convex the deformation occurred at the beach. We cannot tell whether the concavity of the coastline alters the stress vectors within the ice or simply puts a greater distance of

land-fast ice between the coast and the pack ice. However, this is a pattern repeated at larger scales along the Chukchi coast where the land-fast ice extends further and remains stable longer along concave segments.

5. ANALYSIS

5.1. Force analysis

The beach ridges built during the ice shove were similar to those observed by Hopkins (1997) in his experiments and models. Although beach deformation is not included in Hopkins' model, we can make a conservative estimate of the average force applied to the ice at the beach using profiles 1 and 2. Assuming a constant ridge porosity, profile 1 represents a gain in potential energy per unit length of ridge of 150 KJ m^{-1}, relative to a presumed state of isostatic equilibrium, whereas profile 2 represents only 95 KJ m^{-1}. The contributions of the gravel berms are assumed negligible. Taking Hopkins' ratio of dissipative to gravitational work of 8.3 ± 1 and dividing by the distance over which energy was expended (20 m), we arrive at average forces of 50–62 kN m^{-1} to build the ridge of profile 1, and 35–44 kN m^{-1} to build the ridge of profile 2. These values are comparable to forces calculated by Kovacs and Sodhi (1980), who assumed that simple sliding accounted for all dissipative losses during events at beaches on the Finnish coast reported by Alestalo and Häikiö (1975).

It should be noted, though, that the values calculated here represent only the forces required to build the ridges and as yet nothing has been said about the rafting, which is assumed to have accommodated 25 m of ice motion seaward of the beach ridges and 50 m of motion offshore in regions E and F. Parmerter (1975) derived a basic analytic model of the initiation of the rafting process based on two floes converging and behaving as beams on elastic foundations while afloat. Taking typical values for the tensile strength, elastic modulus and Poisson's ratio of sea ice, he deduced a maximum sea-ice thickness of 17 cm, above which the ice would form ridges instead of rafting. In this study we saw clear evidence of rafting in ice approximately 1 m thick, and rafting of ice >2 m thick has been observed by Kovacs and Mellor (1974). Parmerter (1975) concedes such events most likely result from variations in ice mechanical properties.

Experiments and simulations carried out by Hopkins and others (1999) suggest that thicker ice can raft provided the ice thickness is highly homogeneous and that rafting is often preceded by ridging until the conditions become right for rafting. These conditions are dependent on the configuration of the ice, requiring the ice be broken and the faces of the converging sheets be angled such that one floe can be pushed down beneath the other. From the aerial photography, rafting appears to have occurred 25 m from the ridge at the beach, where there is no evidence of pre-existing cracks. It is unclear what caused the ice to break at this point, but evidence from elsewhere on the beach (Fig. 10) suggests the ice sheet broke under buckling.

To calculate the forces necessary to create buckles, there are formulations for both elastic behavior and viscous creep buckling. Sanderson (1988) dismisses elastic buckling of ice <0.5 m thick, and puts forward a theoretical treatment for creep buckling. However, since the majority of the 45 m of motion occurred within a 3 hour period we calculate mean ice velocities of 360 m d^{-1}. This is approximately 3 orders of

Fig. 10. Evidence that the ice failed through buckling. The stick is ~2.4 m long marked at 0.2 m intervals.

magnitude greater than the typical ice velocity of 0.5 m d^{-1} used by Sanderson as well as by Hoyland and Löset (1999) who applied creep buckling to ice deformation in Spitsbergen, Svalbard, where a glacier was encroaching into first-year ice at a rate of 0.2 m d^{-1}. A comparison of viscous and elastic behavior in buckling follows.

Sanderson (1988) lays out the workings to derive the following expression for the effective stress, $\bar{\sigma}$, in terms of half-wavelength of buckles produced, λ_0, ice thickness, h, the density of sea water, ρ_{sw} and acceleration due to gravity, g:

$$\bar{\sigma} = \frac{2\rho_{sw} g}{h}\left(\frac{\lambda_0}{\pi}\right)^2. \quad (3)$$

Taking $\rho_{sw} = 1030$ kg m^{-3}, $g = 9.81$ m s^{-2} and $h = 1$ m, and a buckling wavelength of 25 m, coinciding with where the ice is assumed to have failed prior to rafting, we obtain a stress estimate of 320 kPa and a force per unit length of 320 KN m^{-1}.

For elastic buckling, we can use formulae for the critical stress, σ_c, required to instigate buckling, and the wavelength of the buckles produced, λ_c (Turcotte and Schubert, 1982):

$$\sigma_c = \left(\frac{Eh\rho_{sw} g}{3(1-\nu^2)}\right)^{\frac{1}{2}}, \quad (4)$$

$$\lambda_c = 2\pi\left(\frac{Eh^3}{12(1-\nu^2)\rho_{sw} g}\right)^{\frac{1}{4}}, \quad (5)$$

where E is Young's modulus, ν is Poisson's ratio, h is ice thickness and ρ_{sw} is the density of the sea water. We can take $\nu = 0.3$ and $\rho_{sw} = 1030$ kg m^{-3} as typically used in the literature (e.g. Parmerter 1975; Hopkins and others, 1999). Values for E found in the literature range between 10^8 and 10^{10} Pa, which yield buckling stresses of 0.6–6 MPa.

Using work by Kovacs (1997), a lower-bound estimate of the bulk (full ice-sheet thickness) brine volume fraction and the corresponding bulk horizontal compressive strength can be estimated as 11.8% and 1.1 MPa respectively, assuming a strain rate on the order of 10^{-4} s^{-1} from Figure 6. This is somewhat weaker than values of 1.5–2 MPa put forward by other authors from small-scale tests and extrapolated for ice around -2°C with high brine volumes (Schwarz and Weeks, 1977; Vaudrey, 1977; Timco and Frederking, 1990). This shows that ice with a Young's modulus in the 0.6–6.0 MPa range (also calculated from small-scale

tests) is unlikely to buckle before it crushes. Furthermore, the buckling wavelengths corresponding to the critical buckling stresses above are 110 and 35 m respectively. However, if we invert the problem and assume a buckling wavelength of 25 m, we get a buckling stress of 310 kPa, implying a mean force per unit length of 310 kN m^{-1}, very close to those calculated applying creep buckling theory. The corresponding Young's modulus is around 3×10^7 Pa, which is less than values typically chosen for first-year ice. Instead we have empirically derived an effective modulus which takes some account of the non-elastic properties of sea ice near its melting point where the brine volume fraction becomes highly non-linear with temperature. This demonstrates that creep behavior can be closely approximated by using a low effective modulus in an elastic treatment, which raises questions about what microstructural mechanisms are responsible this behavior.

For a sea-ice temperature of -2°C and a brine volume fraction of 11.8%, an upper-bound estimate of the tensile strength of the ice is around 1.3×10^5 Pa (Dykins, 1970, as cited in Schwarz and Weeks, 1977; Vaudrey, 1977). It can be shown that fiber stresses in the ice exceeding this can be created for small buckling amplitudes of around 0.5 m for buckling wavelengths of 25 m.

Once the ice sheet is broken, if the faces of the ice are not vertical, the advancing ice sheet is then able to raft. This process initially requires force to bend the two sections of the ice sheet and submerge one beneath the other. If we assume the ice to have broken along a straight line producing two near-vertical edges, applying the results of Parmerter (1975) to 1 m thick ice that shows the force required to bend and submerge one portion of the ice sheet is limited to around 64 kN m^{-1}.

Once in this configuration, the submerged sheet is held down by the weight of the sheet on top, and sliding friction dominates resistance to motion. The force per unit length of rafting required to overcome this, F_{sl}, is dependent on the area of contact between the two ice sheets and is given by:

$$F_{\mathrm{sl}} = \mu \rho_{\mathrm{i}} g h L \qquad (6)$$

where μ is the coefficient of friction between the two ice sheets, ρ_{i} is the density of sea ice, taken to be 920 kg m^{-3}, h is ice thickness and L is the distance over which one ice sheet has overridden the other. Kennedy and others (2000) studied the variation of friction coefficients with sliding velocity for bare ice, finding that μ decreases with increasing sliding velocity. The sliding velocity of the ice during the shove was not explicitly observed, although the majority of the estimated 45 m of total motion that occurred on 18 June took place in <3 hours (Table 1). This suggests a minimum ice velocity of around 0.4 cm s^{-1}, though the ice movement is likely to have been discontinuous and faster during the episodes of motion, as observations of other ice shoves (Brower, 1960) suggest. The results of Kennedy and others (2000) then give an upper estimate of $\mu = 0.08$, though it should be noted their work was conducted on ice at -10 °C and did not account for the presence of a lubricating layer of disintegrated friable ice that would be expected for warmer ice (personal communication from A. Kovacs, 2003). Therefore, with an assumed 25 m of rafting at the beach in regions A and B, the maximum sliding force is 18 kN m^{-1}.

From all the force values calculated above, it is apparent that stresses in the ice sheet were highly variable in time, building up prior to failure and rafting, which allow the release of stress. This is in agreement with measurements of stress during ice deformation reported by Tucker and others (1992) and Hopkins (1997). The stresses were also likely to be variable spatially, with processes acting to concentrate stress locally where different sections of ice moved different amounts or encountered different beach slopes (Shapiro and others, 1984). Though it is difficult to weight these values in space and time, the ridge-building forces represent an adequate mean force acting on the ice during the *ivu*.

5.2. Initiation of ice motion

As mentioned earlier, the occurrence of an ice shove is the result of the interplay of many different mechanisms and processes. The most significant occurrences of onshore ice motion coincided with onshore winds, from between the north and west, on 14 and 18 June. On 18 June, the wind speeds during the 3 hour period of ice motion were the highest recorded during that period of onshore winds. It is worth noting here that a similar event was reported at the same time at the village of Wainwright, some 150 km further southwest along the Chukchi coast, where the local winds throughout June and the coastal aspect were similar to those of Barrow. Wind stress on the ice would therefore appear to be one forcing mechanism and a good starting point for the following analysis of the processes responsible for initiating ice motion in the littoral zone.

Hourly averaged wind data are available for Barrow Wiley-Post Airport weather station through the U.S. National Weather Service. These are illustrated in Figure 3, which shows that onshore winds preceded and accompanied ice motion on both 14 and 18 June (see Table 1). The wind blew consistently onshore for nearly 24 hours from 2100 h on 13 June (Fig. 3), with weighted average velocities of 4.4 m s^{-1} from 86° west of north in the range 2.6–6.1 m s^{-1}. After this, the winds were generally stronger, up to 8.7 m s^{-1}, but blowing offshore until approximately 0400 h on 17 June. At this time, a more sustained period of onshore winds began, lasting until nearly 0600 h on 20 June (Fig. 3), with weighted average velocities of 4.6 m s^{-1} from 81° west of north in the range 2.3–7.6 m s^{-1}.

We can estimate the force imparted to the ice from the wind during ice motion on 14 and 18 June using measurements of the wind speed and the fetch of ice and an estimate of the atmospheric drag coefficient. Wind stress on a surface, τ, can be expressed by the equation:

$$\tau = \rho_{\mathrm{a}} C_{\mathrm{d}} {u_z}^2 \qquad (7)$$

where ρ_{a} is the density of air, C_{d}, is the drag coefficient and u_z is the wind velocity at height z above the surface, which is typically taken at 10 m. Many authors (e.g. Arya, 1973; Banke and Smith, 1973; Banke and others, 1980; Macklin, 1983; Anderson, 1987) have derived formulas and made calculations for drag coefficients, which are found to depend strongly on the surface characteristics of the ice.

Arya (1973) and Banke and others (1980) give formulas for calculating C_{d} in terms of skin drag and form drag, but detailed knowledge of the long-range surface roughness characteristics is required, which is unavailable for this study. The aerial-photography coverage does not extend far offshore, but observations during the flights over the ice suggested that the ice became very rough 1–2 km from shore, with areal fractions of hummocked or ridged ice $>50\%$. The state of the sea ice offshore from Barrow has not been

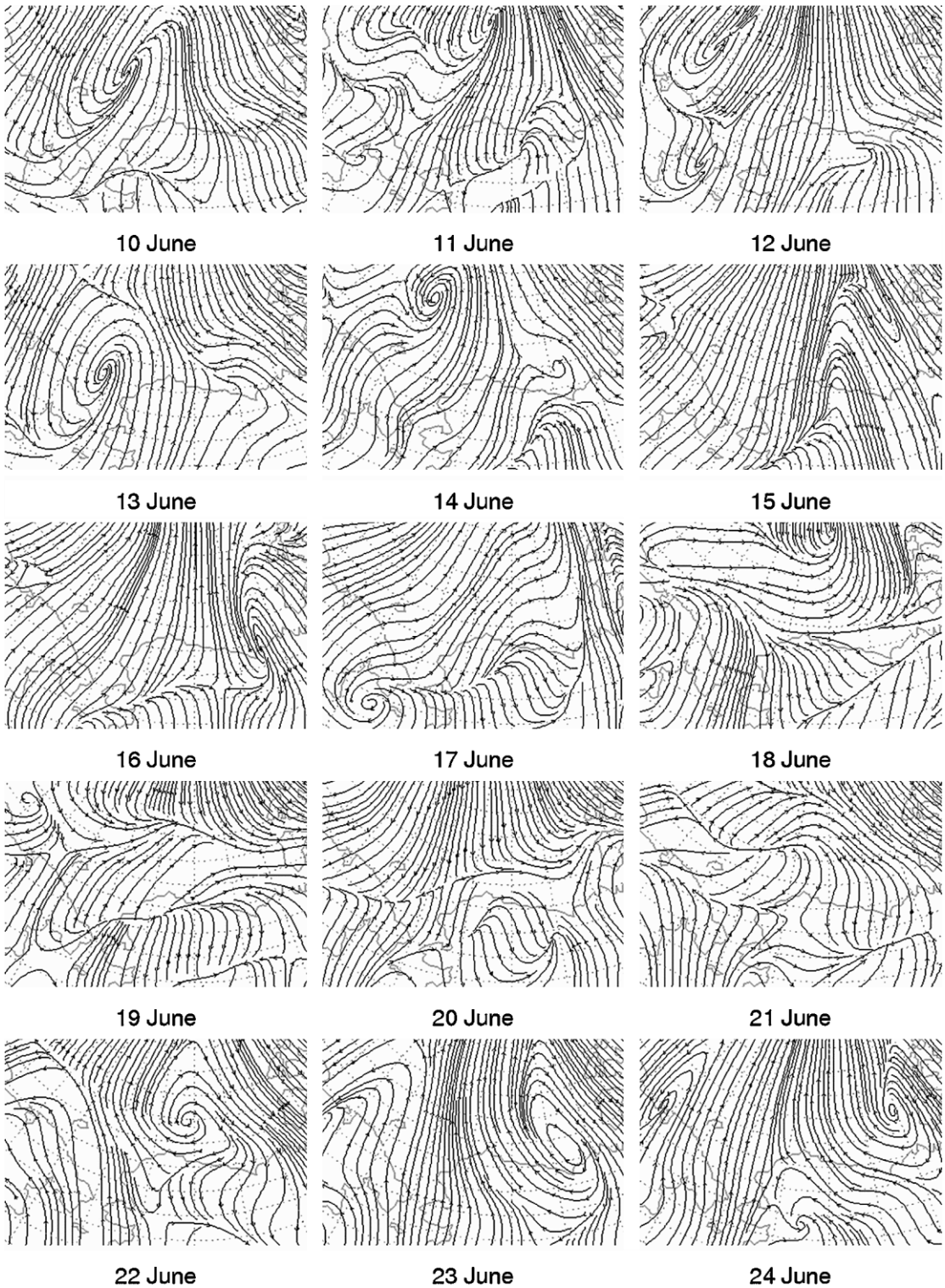

Fig. 11. NCEP re-analysis data showing daily averaged wind fields in the region of the Chukchi Sea. From 10 to 17 June, the Chukchi Sea experienced consistent southerly winds, leading to sea-ice compaction against the perennial ice to the north. On 18 June, the winds changed to blow against the Alaskan Chukchi coast, coinciding with the day of most sea-ice deformation at the beach in Barrow.

well observed at this time of year, but recent observations from the USCG Healy in this area (Eicken, unpublished data) suggest comparable roughness offshore.

Macklin (1983) compiled a table of drag coefficients over sea ice, listing values given by previous authors, and found a range of between 0.001 over smooth, flat ice and his own measurement of 0.003 over heavily fractured 1 m thick floes with numerous small rubble piles. Taking this description to fit what we know of the sea offshore of Barrow at the time of the ice shove, this latter value seems suitable.

During the period 14–18 June, the temperature, relative humidity and air pressure remained relatively constant, so variation in air density was small, allowing us to assume a constant value of 1.3 kg m^{-3}. Taking the mean wind speed on 18 June gives an estimate of the wind stress on the ice of 0.085 Pa. This suggests that a fetch of 730 km was required for sufficient wind stress to be imparted to the ice, taking the maximum estimate of ridge-building forces calculated in section 5.1. Implicit in this calculation is the assumption of a uniform stress field in the absence of evidence of non-

uniformity. The phenomena of non-simultaneous ice failure (Kovacs and Sodhi, 1988), where only discrete parts of the ice sheet are in contact with the ridge, can act to concentrate the stress in small regions and reduce the necessary fetch. However, Kovacs and Sodhi (1988) note that the amplifying effects of this become negligible when failure occurs over distances greater than approximately 2 km. It is not known how the coast between Barrow and Wainwright was affected beyond the view with binoculars from Barrow, but it seems safe to assume that this ice shove was more than a local event.

Although U.S. National Ice Center ice charts and Advanced Very High Resolution Radiometer (AVHRR) imagery show that a continuous sheet of ice of sufficient extent was present offshore from Barrow between 14 and 18 June, we should not expect our local wind velocity measurements and drag coefficients to remain representative over such distances and there are a number of observations that demonstrate the need to consider larger-scale conditions and other processes. For example, the magnitude of ice movement on 14 June was less than that on 18 June, despite the great similarity in the weighted average wind velocities on these two days. Figure 1 shows the closure of the coastal lead and the consolidation of the offshore ice between 8 and 18 June. Although the lead was mostly closed on 14 June, the nearshore pack ice continued to become more compact until 18 June despite offshore winds (Fig. 3). This indicates that the pack ice still possessed shoreward momentum. Momentum transfer from the pack ice is discussed next, but part of the difference in magnitudes of ice motion at the beach between 14 and 18 June may be due to the less consolidated pack ice on 14 June being less able to transfer wind stress to the coast. Other observations suggest the involvement of mechanisms and processes other than onshore wind stress. Not only did the closure of the coastal flaw provide a continuous extent of ice up to the coast for the wind to blow over and impart stress to the ice, but the act of closing the lead is likely to have imparted momentum to the land-fast ice. The initial impact against the land-fast ice occurred on the same day as the initial movement on 14 June, but it seems unlikely that impact forces contributed to the ice motion at the beach on 18 June.

The continued compaction of the pack ice and modest deformation at the beach despite local offshore winds until 18 June indicate that the pack ice was being forced shoreward by processes distant from the coast. Daily averaged 10 m wind fields from U.S. National Centers for Environmental Prediction (NCEP) re-analysis data (Fig. 11) show that between 10 and 17 June the wind was consistently blowing northward in the southern Chukchi Sea. This wind pattern will have led to compaction of sea ice in the central Chukchi Sea, which is seen in the AVHRR data and caused pack ice, with nowhere else to go, to move into any available open-water region. The closing of the coastal flaw lead near Barrow against local offshore winds is therefore likely to be caused by pack-ice stress as the sea ice of the Chukchi Sea was compacted against the perennial pack ice to the north.

The NCEP data for 18 June show northwesterly winds in the central Chukchi Sea, blowing toward the Alaskan Chukchi Sea coast over a distance of several hundred kilometers, before resuming a general southerly flow on 19 June. Therefore the locally measured winds at Barrow on 18 June (Fig. 3) may have been representative of the wind over a sufficient fetch of continuous sea ice to initiate shoreward motion of the land-fast ice. If not, then it is likely that stresses related to the compaction of the pack ice and closure of the coastal flaw lead contributed to the event. Either way, it is apparent that both mechanisms were necessary to close the coastal flaw lead and impart ice stress to the shore. This is supported by the lack of ice shoves on other occasions during spring 2001, when only one of the above mechanisms was acting. There were strong, sustained onshore winds earlier in April and May that did not result in ice shoves. Around 20 May, onshore winds occurred, but the coastal flaw lead remained mostly open according to AVHRR imagery, and an ice shove did not occur.

It is also likely that some preconditioning of the land-fast ice reduced the amount of force necessary for an ice shove. Between 30 March and 2 April, before the onset of melting, no ice shoves occurred despite a closed flaw lead and greater wind forcing than on 14 and 18 June (onshore winds reached 12.3 m s^{-1}, averaging 9.1 m s^{-1}). This suggests that warming of the ice before 14 June, which led to melting of the bottom-fast ice zone and a reduction in ice strength and stiffness, was another factor in this coastal ice shove. However, as discussed earlier, ice shoves have been observed at all times during the ice season and so other mechanisms must be active to incur ice shoves in colder, stronger, better-anchored land-fast ice.

It is certain that other processes must act to destabilize the ice for ice shoves to occur at other times of year, but it is not necessary that these are coincident with the action of onshore forcing from pack ice and winds. In recent years, Barrow has seen a number of wintertime ice breakout events, leaving open water at the beach. These events are likely to be related to a shortening of the stable period of Alaskan land-fast ice, as suggested by AVHRR and ground observations for the period 1998–2001 (Mahoney and others, unpublished information), and will result in a less stable ice cover in the remaining months of the land-fast ice year. Ice shoves similar in magnitude to and smaller than the one studied here have occurred on the Alaskan Chukchi coast each spring in the 2000–02 interval, and it is possible that, with less stable land-fast ice, more events may occur in the future.

The full RADARSAT SAR scenes used to produce Figure 1 show that pack-ice motion was approximately parallel to the shore in a northeasterly direction between 14 and 18 June. This is likely to have produced a large amount of shear against the stationary land-fast ice and is probably responsible for the northeast–southwest feature near the coast in Figure 1d, which is interpreted as a shear ridge. Water drag from ocean currents beneath the land-fast ice may also have contributed to this ice motion, but flow parallel to the coast is unlikely to have contributed a significant onshore stress. The sea-surface slope associated with such currents may lift grounded floes from the seabed, allowing the land-fast ice to move, but hydrographic measurements supporting this are not available.

6. CONCLUSIONS

At least 140 m of shoreward land-fast ice motion at the beach was accommodated almost entirely in narrow linear ridges so that little or no onshore ride-up occurred. Further offshore, up to 395 m was accommodated mostly in a manner

inferred to be finger rafting, an exceptional phenomenon for ice <1 m thick.

We have identified four key factors responsible for initiating motion of land-fast ice in June 2001:

1. Compaction of sea ice in the central Chukchi Sea over a period of up to a week
2. Closure of the coastal flaw lead (possibly a consequence of 1)
3. Onshore winds, around 4 m s^{-1}
4. Warming of the land-fast ice, leading to a reduction in strength and stability.

Movement and deformation of the land-fast ice was strongly associated with the occurrence of onshore winds, which were measured locally and apparently acted over several hundred kilometers offshore. However, other processes must have been acting up to a week beforehand to close the coastal flaw lead and set up a sufficient combination of fetch and shoreward pack-ice stress. Pack-ice motion near the northern Alaskan Chukchi coast did not correlate with local winds, and the coastal flaw lead closed while the winds were offshore. This seems to be the complex response of sea ice in the central Chukchi compacting into the perennial ice to the north under the influence of prolonged southerly winds.

Another crucial factor in this event appears to be the thermal regime of the ice, which was above −2°C throughout and by inference had a very low mechanical strength. This is likely to have been responsible for allowing the 1 m thick ice to raft and reducing the amount of force required to overcome the resisting forces anchoring the land-fast ice. The implications of this extend beyond the occurrence of ice shoves to encompass all summertime sea-ice deformation, where the occurrence of rafting and the associated ice thickening may be an under-observed phenomenon. In failing to consider deformation of warm, summertime ice, sea-ice dynamic models may be overlooking a mechanism of deformation and thickness redistribution.

The effect of local bathymetry and coastal morphology in modulating the response of the ice to the onshore forcing was illustrated well in this event. The motion-vectors fields show that a submarine shoal within approximately 500 m of the beach prevented ice deformation at the beach behind it and possibly reduced deformation at the beach further up the coast. In addition, there was evidence that the curvature of the coast may influence the proximity of the deformation to the beach. If further work bears out such relationships, then perhaps some sections of coastline are more sensitive than others to ice shoves. Taking this further, if sediment reworking by ice shoves is significant for coastal processes, then there may be feedbacks to coastal morphology and such events may play a role in shaping Arctic coastlines.

While the ice shove near Barrow in June 2001 provided an excellent opportunity to document and study the processes and mechanisms involved in an *ivu* event, the impact upon the local community and coast regime was only slight. There were no reports of damage to property or infrastructure, and the amount of sediment reworking was negligible. There was no evidence of the ice shove by the following fall. However, the potential impacts were high, with houses, roads and powerlines lying within 50 m of the water's edge, significantly less than the overall distance moved by parts of the land-fast ice. With an increasing interest in nearshore development in the Arctic, this highlights the usefulness of prediction of such events, which may become more frequent if observed changes in land-fast sea-ice behavior persist.

ACKNOWLEDGEMENTS

We would like to gratefully acknowledge logistics support from the Barrow Arctic Science Consortium and thank T. George for the flights and J. Richter-Menge, D. Perovich and K. Frey for help in the field. A. Kovacs, D. Sodhi and E. Kempema provided many helpful suggestions and improvements as referees, as did M. Lange as Scientific Editor. This work was made possible by a grant from the U.S. National Science Foundation (NSF-OPP-9910888).

REFERENCES

Alestalo, J. and J. Häikiö. 1975. Ice features and ice-thrust shore forms at Luodonselkä, Gulf of Bothnia, in winter 1972/73. *Fennia* 144.

Anderson, R. J. 1987. Wind stress measurements over rough ice during the 1984 marginal ice zone experiment. *J. Geophys. Res.*, **92**(C7), 6933–6941.

Arya, S. P. S. 1973. Contribution of form drag on pressure ridges to the air stress on Arctic ice. *J. Geophys. Res.*, **78**(30), 7092–7099.

Banke, E. G. and S. D. Smith. 1973. Wind stress on Arctic sea ice. *J. Geophys. Res.*, **78**(33), 7871–7883.

Banke, E. G., S. D. Smith and R. J. Anderson. 1980. Drag coefficients at AIDJEX from sonic anemometer measurements. *International Association of Hydrological Sciences Publication* 124 (Symposium at Seattle 1977 — *Sea Ice Processes and Models*), 430–442.

Brower, C. D. 1960. *Fifty years below zero: a lifetime of adventure in the Far North.* New York, Dodd, Mead Co. (in collaboration with P. J. Farrelly and L. Anson)

Dykins, J. E. 1970. *Ice engineering: tensile properties of sea ice grown in a confined system.* Port Hueneme, CA, Naval Civil Engineering Laboratory. (NCEL Technical Report R680.)

Eicken, H., T. C. Grenfell, D. K. Perovich, J. A. Richter-Menge and K. Frey. 2004. Hydraulic controls of summer Arctic pack ice albedo. *J. Geophys. Res.*, **109**(C08007). (10.1029/2003JC001989.).

Flato, G. M. and W. D. Hibler, III. 1995. Ridging and strength in modeling the thickness distribution of Arctic sea ice. *J. Geophys. Res.*, **100**(C9), 18,611–18,626.

Hopkins, M. A. 1994. On the ridging of intact lead ice. *J. Geophys. Res.*, **99**(C8), 16,351–16,360.

Hopkins, M. A. 1997. On-shore pile-up: a comparison between experiments and simulations. *Cold Reg. Sci. Technol.*, **26**(3), 205–214.

Hopkins, M. A., J. Tuhkuri and M. Lensu. 1999. Rafting and ridging of thin ice sheets. *J. Geophys. Res.*, **104**(C6), 13,605–13,613.

Hoyland, K.V. and S. Löset. 1999. Monitoring and observation of the formation of a first-year ice ridge-field. *In* Tuhkuri, J. and K. Riska, *eds. POAC'99, Proceedings of the 15th International Conference on Port and Ocean Engineering under Arctic Conditions, Espoo, Finland, August 23–27, 1999, vol. 1.* Helsinki, Helsinki University of Technology, Ship Laboratory, 37–48.

Kennedy, F. E., E. M. Schulson and D. E. Jones. 2000. The friction coefficient of ice on ice at low sliding velocities. *Philos. Mag.* A, **80**(5), 1093–1110.

Kovacs, A. 1997. Estimating the full-scale flexural and compressive strength of first-year sea ice. *J. Geophys. Res.*, **102**(C4), 8681–8689.

Kovacs, A. and M. Mellor. 1974. Sea ice morphology and ice as geologic agent in the southern Beaufort Sea. *In* Reed, J. C. and J. E. Sater, *eds. The coast and shelf of the Beaufort Sea.* Arlington, VA, Arctic Institute of North America, 113–161.

Kovacs, A. and D. S. Sodhi. 1980. Shore ice pile-up and ride-up: field observations, models, theoretical analysis. *Cold Reg. Sci. Technol.*, **2**, 209–288.

Kovacs, A. and D. S. Sodhi. 1988. Onshore ice ridge-up and pile-up: observations from theoretical assessment. *In* Chen, A. T. and P. Leidersdorf, *eds. Arctic coastal processes and slope protection.* Reston, VA, American Society of Civil Engineers. ASCE Technical Council on Cold Regions, 108–142.

Macklin, S. A. 1983. Wind drag coefficients over first year sea ice in the Bering Sea. *J. Geophys. Res.*, **88**(C5), 2845–2852.

Parmerter, R. R. 1975. A model of simple rafting in sea ice. *J. Geophys. Res.*, **80**(15), 1948–1952.

Parmerter, R. R. and M. D. Coon. 1972. Model of pressure ridge formation in sea ice. *J. Geophys. Res.*, **77**(33), 6565–6575.

Reimnitz, E., P.W. Barnes and J. R. Harper. 1990. A review of beach nourishment from ice transport of shoreface materials, Beaufort Sea, Alaska. *J. Coast. Res.*, **6**(2), 439–470.

Sanderson, T. J. O. 1988. *Ice mechanics: risks to offshore structures.* London, Graham and Trotman.

Schwartz, J. and W. F. Weeks. 1977. Engineering properties of sea ice. *J. Glaciol.*, **19**(81), 499–531.

Shapiro, L. H., R. C. Metzner, A. Hanson and J. B. Johnson. 1984. Fast ice sheet deformation during ice-push and shore ice ride-up. *In* Barnes, P.W., D.M. Schell and E. Reimnitz, *eds. The Alaskan Beaufort Sea: ecosystems and environments.* Orlando, FL, Academic Press, 137–157.

Sodhi, D. S., K. Hirayama, F. D. Haynes and K. Kato. 1983. Experiments on ice ride-up and pile-up. *Ann. Glaciol.*, **4**, 266–270.

Thorndike, A. S. 1986. Kinematics of sea ice. *In* Untersteiner, N., *ed. Geophysics of sea ice.* London, etc., Plenum Press, 489–549.

Timco, G.W. and R. M.W. Frederking. 1990. Compressive strength of sea ice sheets. *Cold Reg. Sci. Technol.*, **17**(3), 227–240.

Tucker, W. B., III, and D. K. Perovich. 1992. Stress measurements in drifting pack ice. *Cold Reg. Sci. Technol.*, **20**(2), 119–139.

Turcotte, D. L. and G. Schubert. 1982. Geodynamics: applications of continuum physics to geological problems. New York, etc., John Wiley and Sons.

Vaudrey, K. D. 1977. *Ice engineering: study of related properties of floating sea-ice sheets and summary of elastic and viscoelastic analyses.* Port Hueneme, CA, Naval Construction Battalion Center. Civil Engineering Laboratory. (Technical Report R860.)

MS received 4 February 2003 and accepted in revised form 4 January 2004